Research Article Vol. 27, No. 14 | 8 Jul 2019 | OPTICS EXPRESS 19233
Optics EXPRESS

Single photon MIR upconversion detector at room temperature with a PPLN ridge waveguide

LUCIEN LEHMANN,[1,*] LUDOVIC GROSSARD,[1] LAURENT DELAGE,[1] FRANCOIS REYNAUD,[1] MATHIEU CHAUVET,[2] AND FLORENT BASSIGNOT[3]

[1] *Univ. Limoges, CNRS, XLIM, UMR 7252, F-87000 Limoges, France*
[2] *FEMTO-ST Institute, UMR CNRS 6174, Université de Bourgogne Franche-Comté, 25000 Besançon, France*
[3] *Femto-Engineering, 15B avenue des Montboucons, 25000 Besançon, France*
[*] *lucien.lehmann@xlim.fr*

Abstract: In this paper we describe an upconversion detector in the mid infrared (around 3.5 µm). We take advantage of the PPLN ridge waveguide technology to achieve single photon detection at room temperature on a single spatial mode. With a pump power of 192 mW we obtain a detection efficiency of 0.4% for 22k dark count per second, which corresponds to a noise equivalent power of 3.0 fW $\cdot$ Hz$^{-1/2}$ and an internal conversion efficiency of 85 %/W of pump.

1. Introduction

The mid-infrared (MIR) spectral domain (3 µm to 5 µm) is a region of interest for a wide range of applications such as spectroscopy, astronomy, environment monitoring, free space communication [1, 2]. However some of these applications require low flux detection that heavily relies on complex cryogenic detectors, like superconducting nanowire single photon detectors (SNSPDs) [3] or HgCdTe avalanche photodiodes [4]. These cryogenic systems are mandatory both to operate MIR detectors and to reduce the background radiation which is a limiting factor in most applications.

In the last decade, upconversion detection has emerged as a promising alternative technique for single-photon detection in the MIR at room temperature. An upconversion detector is based on the Sum Frequency Generation (SFG) non-linear process to frequency shift an optical signal from the MIR domain to the near infrared (NIR) using an intense pump laser. The converted signal can then be optically processed using widely available NIR optical components before being detected by efficient single photon detectors, typically Silicon avalanche photodiodes (SiAPD). This upconversion process selects a limited number of spatial and spectral modes in the surrounding environment, significantly reducing the impact of the background radiation.

Two types of non-linear crystals have been used in the framework of upconversion detectors: bulk crystals and waveguides. Bulk crystals have been used in two different pumping configurations: single pass and resonant cavity. The former has a lower conversion efficiency [5] than the latter [6] but could be more appropriate for some phase dependent optical processing, like coherence analysis by interferometry [7, 8]. On the other hand, non-linear waveguides are viable alternatives to obtain coherent upconversion with good conversion efficiency [9]. Among the different waveguide technologies currently available, the ridge technology is one of the most promising. It offers a significantly better overlapping of the confined fields for very different wavelengths and a better stability at high pump power compared to Ti-indiffused [9] or Reverse Proton Exchange waveguides [10].

In order to investigate the potential of this technology, we built an upconversion detector based on a PPLN ridge waveguide, and fully characterized it in terms of conversion efficiency and noise in the photon counting regime. This characterization was performed using a thermal source

#365903 https://doi.org/10.1364/OE.27.019233
Journal © 2019 Received 25 Apr 2019; revised 22 May 2019; accepted 28 May 2019; published 24 Jun 2019

Optics EXPRESS

emitting in the femtowatt range on a single spatial mode in the MIR.

In Section 2, we will briefly recap the theoretical background of the SFG process. In Section 3, we will describe the design and fabrication of the PPLN ridge waveguide. In Section 4, we will show the experimental setup. In Section 5, we will detail the data processing. And finally, in Section 6 and 7, we will present the main experimental results and a noise analysis of the single-photon MIR upconversion detector.

2. Theoretical description of the SFG process

In a second-order nonlinear material, the copropagation of a signal and a pump field, at frequency ν_s and ν_p respectively, locally generates a converted field at frequency ν_c such that $\nu_c = \nu_p + \nu_s$. In order to obtain a significant conversion efficiency, the wavelets produced throughout the nonlinear crystal have to constructively interfere. In a PPLN waveguide, optimal constructive interference is obtained when the quasiphase matching condition is satisfied, namely:

$$\Delta k = \frac{2\pi n_s \nu_s}{c} + \frac{2\pi n_p \nu_p}{c} - \frac{2\pi n_c \nu_c}{c} - \frac{2\pi}{\Lambda} = 0, \tag{1}$$

where Λ is the poling period, c the speed of light in a vacuum and n_i $(i = s, c, p)$ are the effective refractive indices of the guided mode at the frequency ν_i. In a ridge waveguide, the effective refractive indices depend on the frequency but also on the temperature and the geometry of the waveguide.

The deviation from the quasiphase matching condition leads to a decrease of the conversion efficiency $\eta(\Delta k)$ according to the equation [10]:

$$\eta(\Delta k) = \frac{N_c}{N_s} = \eta_{\text{nor}} P_{\text{pump}} L^2 \,\text{sinc}^2\left(\frac{\Delta k L}{2}\right), \tag{2}$$

with N_s and N_c the number of photons at the signal and the converted frequency respectively, P_{pump} the pump power coupled in the waveguide, L the length of the waveguide and η_{nor} the normalized conversion efficiency (in $\text{W}^{-1} \cdot \text{m}^{-2}$) given by:

$$\eta_{\text{nor}} = \frac{1}{A_{\text{eff}}} \left(\frac{8\pi^2 \nu_s \nu_c d_{\text{eff}}^2}{n_s n_p n_c c^3 \epsilon_0}\right), \tag{3}$$

where ϵ_0 is the vacuum permittivity, d_{eff} the effective nonlinear coefficient and A_{eff} the effective area of the waveguide. Assuming the guided modes have similar profiles equated to a circular Gaussian with a waist w, we can then infer that $A_{\text{eff}} = w^2 \frac{9\pi}{8}$.

Using the conservation of energy ($\nu_c = \nu_p + \nu_s$) and the definition of Δk, Eq. (2) can be rewritten as:

$$\eta(\nu_c) = \eta_{\text{nor}} P_{\text{pump}} L^2 \,\text{sinc}^2\left(\frac{\pi(\nu_c - \nu_{c0})}{\Delta\nu_c}\right), \tag{4}$$

where ν_{c0} is the converted central frequency and $\Delta\nu_c$ the spectral acceptance of the SFG process.

Assuming this spectral acceptance definition, a broadband MIR source with a spectral flux density B_0 has a theoretical number of converted photons $\int \eta(\nu_c) B_0 d\nu_c = B_0 \eta(\nu_{c0}) \Delta\nu_c$. This allows us to define the system detection efficiency as :

$$DE = N/(B_0 \Delta\nu_c) \tag{5}$$

where N is the measured number of photons converted per second.

Research Article | Vol. 27, No. 14 | 8 Jul 2019 | OPTICS EXPRESS 19235

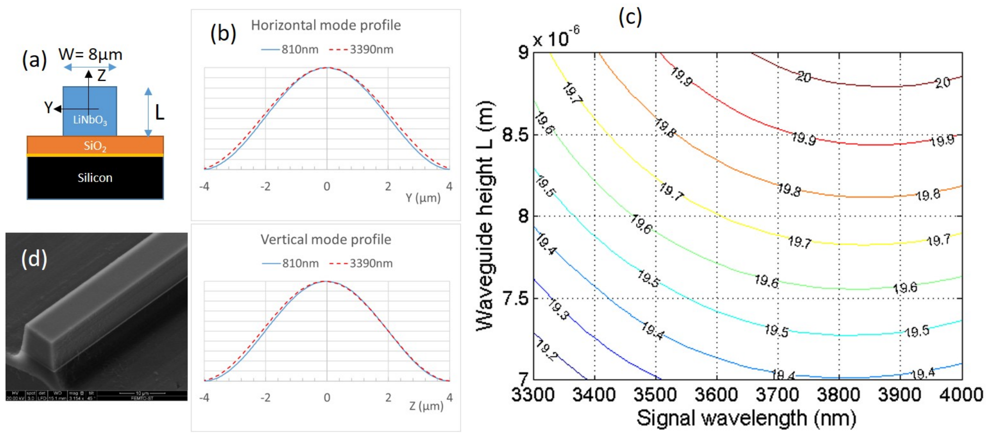

Fig. 1. (a) Schematic waveguide cross section, (b) normalized horizontal and vertical TM_{00} mode profiles for 3390 nm signal and 810 nm SFG, (c) waveguide poling period versus signal wavelength and waveguide height L for SFG with a 1064 nm pump in a 8 µm wide ridge waveguide at 20 °C, (d) SEM image of a fabricated ridge.

3. Design and fabrication of the PPLN ridge waveguide

Several characteristics are fulfilled to optimize the SFG conversion efficiency in a PPLN ridge waveguide. First, the two incident wavelengths (signal and pump) are polarized along the crystal z-axis to benefit from the strongest nonlinear coefficient d_{33} of $LiNbO_3$. Second, a square 8×8 µm^2 waveguide cross section (see Fig. 1(a)) is targeted as a compromise to both facilitate light coupling with a circular Gaussian beam and to obtain a strong confinement. In addition, the high index contrast between the $LiNbO_3$ core waveguide and the SiO_2 substrate gives fundamental mode profiles that are very similar for wavelengths between MIR and visible wavelengths as witnessed by the calculated modes profiles shown in Fig. 1(b). Lastly, to satisfy the quasiphase matching condition Eq. (1), the $LiNbO_3$ sample is poled with the adequate period Λ. Λ is not only dependent on the wavelengths of the interacting beams but also on the architecture of the waveguide through the effective refractive indices of the modes. The poling period is calculated via Eq. (1) where the effective refractive indices of the modes are calculated with the commercial software COMSOL. The dispersion of the refractive index of congruent $LiNbO_3$ is taken from [11]. Figure 1(c) presents the predicted poling period for a signal wavelength varying between 3300 nm and 4000 nm and a waveguide height between 7 µm and 9 µm and a width of 8 µm at 20 °C for a pump wavelength of 1064 nm . For an ideal 8×8 µm^2 square waveguide and a signal at 3500 nm we thus find that a poling period near 19.6 µm is requested. Note that at the same wavelengths quasi-phase-matching in a bulk $LiNbO_3$ crystal would necessitate a larger 22.3 µm poling period. Under these circumstances, the converted signal produced by the SFG process is 816 nm. The phase matching condition can by slightly tuned by an adjustment of the waveguide temperature thanks to the temperature dependence of $LiNbO_3$ refractive index [11].

The first stage of the fabrication is to periodically pole a 500 µm thick commercial z-cut congruent $LiNbO_3$ wafer, supplied by Gooch & Housego, by a standard technique involving the application of an intense electric field at room temperature [12] using a photo-resist pattern. Several poling periods near 19.6 µm are realized to take into account manufacturing tolerances. In a second stage, a SiO_2 layer is deposited by ICPECVD (Inductively-Coupled Plasma-Enhanced Chemical Vapour Deposition) onto one face of the poled wafer followed by the sputtering of a 100 nm-thick gold layer. A high flatness silicon wafer is also coated with a 100 nm-thick gold layer. The metalized faces of both the PPLN and silicon wafers are then placed into contact and

Optics EXPRESS

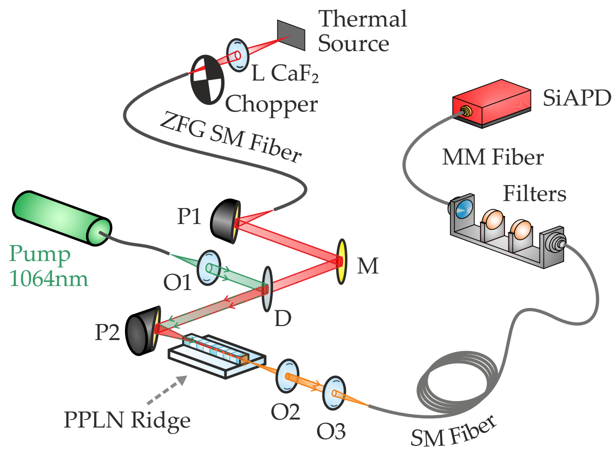

Fig. 2. Scheme of the experimental setup. Px: off axis parabola; L CaF_2: CaF_2 lens; Ox: microscope objectives; D: dichroic mirror (HR@1064 nm; AR@3.5 µm); ZFG SM fiber: ZBLAN fluoride glass single mode fiber; MM fiber: multimode fiber; M: mirror.

pressed in a wafer bonding machine. This metal diffusion bonding process is realized at room temperature which prevents mechanical stress that could occur due to the dissimilar temperature coefficients of the two wafers. Gold was chosen since it is highly ductile and, more importantly, is inert which allows a strong bonding under sole application of pressure. The bonding is completed by applying a strong pressure to the stack which yields more than 98% of the surface bonded as observed by an ultrasound characterization technique. At this stage, a typical 1 mm thick hybrid structure composed of a silicon substrate bonded to a PPLN wafer is obtained. The structure is then thinned down by grinding and polishing techniques to obtain a 8 µm thick PPLN layer. Note that this method was used earlier to produce adhered non-linear ridge waveguides [13–15] where either epoxy glue or direct bonding was used to fix the PPLN wafers onto $LiNbO_3$ or $LiTaO_3$ substrates. In the next step, two parallel trenches are cut in the PPLN by a precision dicing saw to form the lateral sides of the ridge waveguide. The dicing parameters are set to minimize roughness of the cut surfaces [16, 17]. Finally, the hybrid wafer is diced to achieve polished input and output faces for the ridge waveguides. Figure 1(d) presents a Scanning Electron Microscope (SEM) image of a realized waveguide. We observe that both sides of the ridge are curved due the radius of curvature of the blade corner. By optical profilometry a 3-4 nm RMS roughness is measured for the ridge faces. Such a surface quality ensures low propagation losses. No further polishing of the input and output faces is necessary for direct coupling.

The PPLN ridge waveguide used to build the upconversion detector is 20 mm long with a poling period $\Lambda = 19.6\,\mu\text{m}$ and a $8 \times 8\ \mu\text{m}^2$ cross section. At the wavelengths of interest the TM_{00} modes of the waveguide (Fig. 1(b)) can be approximated by a gaussian beam with a waist radius $w = 3\,\mu\text{m}$. Thus, with an effective nonlinear coefficient $d_{\text{eff}} = \frac{2}{\pi} d_{33} = 15\,\text{pm} \cdot \text{V}^{-1}$, the normalized conversion efficiency should be, according to Eq. (3), $\eta_{\text{nor}} \approx 7500\,\text{W}^{-1} \cdot \text{m}^{-2}$ and $\eta_{\text{nor}} L^2 \approx 300\,\%/\text{W}$ of pump.

4. Experimental setup

The PPLN ridge waveguide described in the previous section has been integrated in the upconversion detector. Figure 2 shows the test bench needed to characterize the upconversion detector. It can be divided into three parts: the MIR stage, the SFG stage and the NIR stage. The MIR stage is composed of a MIR thermal source spatially filtered by a ZBLAN fluoride glass (ZFG) single mode fiber. The thermal source is a metallic plate coated with candle soot in order to

Optics EXPRESS

get an emissivity as close as possible to 1. The temperature of this source can be adjusted between $-8\,°C$ and $70\,°C$ in order to produce a tuneable calibrated MIR source emitting between 0.25 and 8.8 $\mathrm{fW \cdot nm^{-1}}$/spatial mode around 3.5 µm on a single linear polarization. The flux emitted by this source is temporally modulated by an optical chopper at a frequency $f_{\mathrm{mod}} = 140\,\mathrm{Hz}$. This modulation allows us to discriminate the converted signal from the noise and improves the detection capability through the data processing described in Sec. 5. However, because the chopper blades are at ambient temperature, they also emit MIR light (1.1 $\mathrm{fW \cdot nm^{-1}}$/spatial mode around 3.5 µm). Therefore we don't directly measure the flux emitted by the thermal source but the differential flux between the thermal source and the chopper blades.

In the SFG stage, the 192 mW emitted by the pump laser at 1064 nm are mixed with the MIR signal by a dichroic mirror. Both are injected into the PPLN ridge waveguide where the SFG process takes place.

At the output of the nonlinear waveguide, the converted signal around 817 nm is collected by a single mode silica fiber and spectrally filtered by three band-pass filters (12 nm wide around 820 nm) in order to remove the remaining pump flux. The single mode fiber is used to preserve the spatial mode selected by the ZFG fiber in the MIR. Finally, the converted flux is detected by an avalanche photodiode (SiAPD) working in the photon counting regime. Besides the converted flux, the photon counting unit also detects a parasite signal generated by unwanted nonlinear effects, whose origin will be detailed in Sec. 7.

5. Data processing

For each temperature of the thermal source, we acquire 1-s long frames that we coherently average between 30 seconds and 4 minutes. These records contain the time of arrival of each detected photon. We call $\widetilde{X}(f)$ the Fourier transform of this average frame. The complex value of $\widetilde{X}(f)$ at the modulation frequency of the chopper f_{mod} can be written as:

$$\widetilde{X}(f_{\mathrm{mod}}) = \frac{1}{2} N_{\mathrm{TS}}.\exp[i\phi_0] + \frac{1}{2} N_{\mathrm{chp}}.\exp[i(\phi_0 + \pi)] \tag{6}$$

where N_{TS} and N_{chp} are the number of detected photons originating from the thermal source and the blades of the optical chopper respectively, and ϕ_0 the phase of the intensity modulated signal of the thermal source. In our experimental configuration, we measure $\phi_0 = -1$ rad. The modulation applied on the signal leads to a 180° phase shift between the signal radiated by the thermal source (blade position: open) and the one emitted by the chopper blades (blade position: closed). Therefore, the measurement is the difference between the thermal source contribution and the chopper blades one:

$$\Delta N = N_{\mathrm{TS}} - N_{\mathrm{chp}} = 2\Re(\widetilde{X}(f_{\mathrm{mod}}).\exp[-i\phi_0]). \tag{7}$$

Assuming both the thermal source and the chopper blades can be described as blackbodies, the measured number of detected photons is compared to a theoretical prediction ΔN_{th} based on the Plank's law in order to calculate the detection efficiency DE of the system as defined by Eq. (5). ΔN_{th} is written as:

$$\Delta N_{th} = DE \cdot \Delta\nu_s (B_{0\mathrm{TS}} - B_{0\mathrm{chp}})/4 \tag{8}$$

$$\Delta N_{th} = \frac{DE \cdot \Delta\lambda_s \cdot \Delta\Omega \cdot \Delta S \cdot \lambda_s}{4hc} \cdot \left[L_{\lambda_s}(T_{\mathrm{TS}}) - L_{\lambda_s}(T_{\mathrm{chp}})\right] \tag{9}$$

$$\Delta N_{th} = \frac{DE \cdot c \cdot \Delta\lambda_s}{2\lambda_s^2} \left(\frac{1}{\exp[\frac{hc}{\lambda_s k_B T_{\mathrm{TS}}}]-1} - \frac{1}{\exp[\frac{hc}{\lambda_s k_B T_{\mathrm{chp}}}]-1} \right), \tag{10}$$

where $B_{0\mathrm{TS}}$ and $B_{0\mathrm{chp}}$ are the flux spectral density emitted by the thermal source and the chopper blades respectively; T_{TS} and T_{chp} are the temperature of the thermal source and the chopper blades respectively; $\Delta\nu_s = c\Delta\lambda_s/\lambda_s^2$ is the spectral acceptance defined by Eq. (4); $\Delta\Omega\Delta S = \lambda_s^2$ is the etendue of a single spatial mode and $L_\lambda(T)$ is the spectral radiance of the blackbody; k_B the Boltzmann constant and h the Planck constant. The factor 4 in Eq. (8) is due to the chopping (50% duty cycle) and the selection of only one linear polarization of the MIR signal through the SFG process. The detection efficiency calculated this way assumes the emissivity of the thermal source and the chopper is equal to 1 and thus slightly underestimates its true value.

The detection efficiency DE depends on several factors from the thermal source to the SiAPD detector: the global transmission of the MIR stage, the conversion by the SFG process, the optical processing, filtering and detection in the NIR stage. It can be expressed as:

$$DE = \epsilon \cdot T_{\mathrm{MIR}} \cdot \eta(\nu_{c0}) \cdot T_{\mathrm{NIR}} \cdot QE \tag{11}$$

where ϵ is the emissivity of the source, T_{MIR} and T_{NIR} are the transmission of the MIR and NIR stages, before and after the conversion stage respectively, $\eta(\nu_{c0})$ is the peak conversion efficiency defined by Eq. (4) and QE the quantum efficiency of the NIR photon counter. Note that the MIR and NIR transmission coefficients take into account the coupling of the MIR light into the PPLN waveguide and the coupling of the converted signal into the single mode fiber respectively, but not the pump laser coupling efficiency.

6. Experimental results

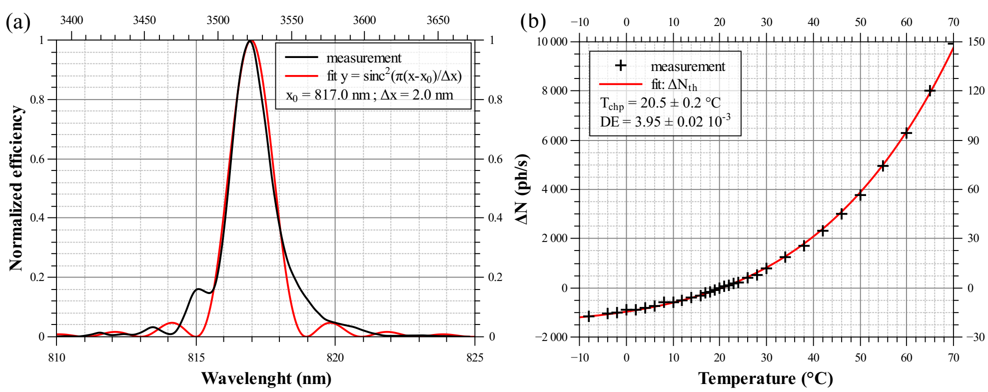

Fig. 3. (a) Conversion spectrum of the SFG process. (b) Differential number of converted photons as a function of the temperature of the thermal source.

The experimental conversion efficiency spectrum of the upconversion detector is plotted in Fig. 3(a). The maximum conversion efficiency is obtained for $\lambda_{c0} = 817.0$ nm ($\lambda_{s0} = 3521$ nm) and the spectral acceptance is equal to $\Delta\lambda_c = 2.0$ nm ($\Delta\lambda_s = 37$ nm). The discrepancy between the experimental curve and the theoretical sinc^2–shape curve is due to variations of the quasi-phase matching condition along the waveguide.

Figure 3(b) shows the differential number of converted photons ΔN experimentally measured as a function of the temperature of the thermal source with 192 mW of pump power.

The experimental curve is fitted by the theoretical model given by Eq. (10) with two degrees of freedom: the detection efficiency DE and the temperature of the chopper blades T_{chp}. The values obtained from this fit are $DE = 3.95 \pm 0.02 \times 10^{-3}$ and $T_{\mathrm{chp}} = 20.5$ °C. The power emitted on a single spatial mode by a blackbody at 20.5 °C on a single polarization is equal to 42 fW (37 nm bandwidth at 3.5 µm).

Assuming $\epsilon = 0.9$, $T_{\mathrm{MIR}} = 0.3$, $T_{\mathrm{NIR}} = 0.35$, $QE = 0.5$ and 50% pump coupling efficiency, we find an internal quantum conversion efficiency equal to 85 %/W of pump, about 30 % of the

Optics EXPRESS

theoretical value for a perfect waveguide (300 %/W of pump). This discrepancy is consistent with the degraded conversion spectrum.

7. Noise analysis

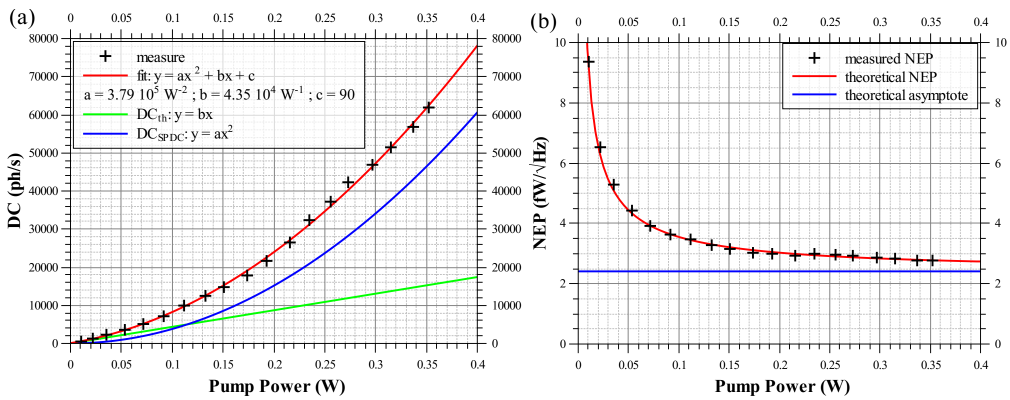

Fig. 4. (a) Evolution of the Dark Count as a function of the pump power. (b) Evolution of the NEP as a function of the pump power. The theoretical NEP and the asymptote are derived from the DC fit shown in Fig. 4(a) and the measured detection efficiency.

Figure 4(a) shows the evolution of the dark count DC as a function of the pump power. These measurements are performed at room temperature with an optical shutter placed between the ZFG fiber and the dichroic mirror. We can discriminate three components:

- a constant component, corresponding to the electronic dark count of the NIR photon counter which is negligible in our case (90 Hz);
- a linear component DC_{th}, corresponding to the conversion of one spatial mode of the thermal background;
- a quadratic component DC_{SPDC}, corresponding to two consecutive nonlinear effects: the production of a signal at 3.5 µm by a SPDC (Spontaneous Parametric Down Conversion) process followed by the conversion of this signal to 817 nm by SFG.

These three components have different impacts on the noise equivalent power (NEP) of the detector. As shown in Fig. 4(b), the NEP of the detector decreases with the pump power toward an asymptote defined as follow:

$$\mathrm{NEP} = \frac{h\nu_s}{DE}\sqrt{2DC} \tag{12}$$

$$= \frac{h\nu_s}{\alpha P}\sqrt{2(aP^2 + bP + c)} \tag{13}$$

$$\xrightarrow[P\to+\infty]{} \frac{h\nu_s\sqrt{2a}}{\alpha} \tag{14}$$

where P is the pump power, $DC = aP^2 + bP + c$ and $\alpha = DE/P$ is the detection efficiency per watt of pump. This asymptote only depends on the quadratic components of the dark count. The constant and linear components only impact the convergence speed. In our case, the value of this asymptote is equal to $2.4\,\mathrm{fW}\cdot\mathrm{Hz}^{-1/2}$.

At 192 mW of pump power, the dark count is equal to 22 kHz, which corresponds to a NEP of $3.0\,\mathrm{fW}\cdot\mathrm{Hz}^{-1/2}$.

8. Conclusion

In this paper we described a state-of-the-art upconversion detector using a PPLN ridge waveguide. In contrast to most of the existing MIR upconversion detectors, this detector is based on a single pass configuration with a relatively low pump power (192 mW) to achieve single photon counting at room temperature around 3.5 µm. Using a thermal source emitting in the femtowatt range on a single spatial mode within the spectral bandwidth of the detector (37 nm), we have measured a NEP equal to $3.0\,\mathrm{fW}\cdot\mathrm{Hz}^{-1/2}$ with a system detection efficiency close to 0.4% and 22kHz dark count rate. These results could be improved as the maximum theoretical value for the internal conversion efficiency is not yet reached. Furthermore several parts of the global design could be refined. For instance, depositing an anti-reflection coating on both ends of the waveguide would significantly increase the transmission of the system and a pigtailed PPLN [18] output would enhance the coupling of the converted signal into the optical fiber.

Funding

Centre National de la Recheche Scientifique (CNRS) (DEFI Instrumentation aux limites 2018, ASHRA INSU 2018); Centre National d'Études Spatiales (CNES) (R&T R-S16/SU-0002-042 2016); Agence nationale de la recherche (ANR) (ANR-15-IDEX-03); Thales Alenia Space.

Acknowledgments

This work has been supported by the Centre National d'Études Spatiales (CNES), Thales Alenia Space, the Institut National des Sciences de l'Univers (INSU). M. Chauvet acknowledges the supports of the French PIA program, project ISITE-BFC (contract ANR-15-IDEX-03). This work was also partly supported by the French RENATECH network and its FEMTO-ST MIMENTO technological facilities.

References

1. A. Rogalski and K. Chrzanowski, "Infrared devices and techniques (revision)," Metrol. Meas. Syst. **21** (2014).
2. C. L. Tan and H. Mohseni, "Emerging technologies for high performance infrared detectors," Nanophotonics **7**, 169–197 (2018).
3. F. Marsili, F. Bellei, F. Najafi, A. E. Dane, E. A. Dauler, R. J. Molnar, and K. K. Berggren, "Efficient single photon detection from 500 nm to 5 μm wavelength," Nano Lett. **12**, 4799–4804 (2012).
4. X. Sun, J. B. Abshire, J. D. Beck, P. Mitra, K. Reiff, and G. Yang, "HgCdTe avalanche photodiode detectors for airborne and spaceborne lidar at infrared wavelengths," Opt. Express **25**, 16589 (2017).
5. G. Temporão, S. Tanzilli, H. Zbinden, N. Gisin, T. Aellen, M. Giovannini, and J. Faist, "Mid-infrared single-photon counting," Opt. Lett. **31**, 1094 (2006).
6. M. Mancinelli, A. Trenti, S. Piccione, G. Fontana, J. S. Dam, P. Tidemand-Lichtenberg, C. Pedersen, and L. Pavesi, "Mid-infrared coincidence measurements on twin photons at room temperature," Nat. Commun. **8**, 15184 (2017).
7. P. Darré, L. Lehmann, L. Grossard, L. Delage, and F. Reynaud, "Control of the coherence behavior in a SFG interferometer through the multipump phases command," Opt. Express **26**, 7098 (2018).
8. L. Lehmann, P. Darré, H. Boulogne, L. Delage, L. Grossard, and F. Reynaud, "Multichannel spectral mode of the ALOHA up-conversion interferometer," Mon. Notices Royal Astron. Soc. **477**, 190–194 (2018).
9. K.-D. F. Büchter, H. Herrmann, R. Ricken, V. Quiring, and W. Sohler, "Waveguide-based mid-infrared up-conversion detectors," in *Advanced Photonics (2011), Paper IWF3,* (Optical Society of America, 2011), p. IWF3.
10. R. V. Roussev, C. Langrock, J. R. Kurz, and M. M. Fejer, "Periodically poled lithium niobate waveguide sum-frequency generator for efficient single-photon detection at communication wavelengths," Opt. Lett. **29**, 1518 (2004).
11. D. H. Jundt, "Temperature-dependent Sellmeier equation for the index of refraction, n_e, in congruent lithium niobate," Opt. Lett. **22**, 1553–1555 (1997).
12. E. Courjon, N. Courjal, W. Daniau, G. Lengaigne, L. Gauthier-Manuel, S. Ballandras, and J. Hauden, "Lamb wave transducers built on periodically poled Z-cut $LiNbO_3$ wafers," Eur. Phys. Journal: Appl. Phys. **102**, 114107 (2007).
13. R. Kou, S. Kurimura, K. Kikuchi, A. Terasaki, H. Nakajima, K. Kondou, and J. Ichikawa, "High-gain, wide-dynamic-range parametric interaction in Mg-doped $LiNbO_3$ quasi-phase-matched adhered ridge waveguide," Opt. Express **19**, 11867–11872 (2011).
14. S. Kurimura, Y. Kato, M. Maruyama, Y. Usui, and H. Nakajima, "Quasi-phase-matched adhered ridge waveguide in $LiNbO_3$," Appl. Phys. Lett. **89**, 191123 (2006).

Optics EXPRESS

15. M. Chauvet, F. Henrot, F. Bassignot, F. Devaux, L. Gauthier-Manuel, V. Pêcheur, H. Maillotte, and B. Dahmani, "High efficiency frequency doubling in fully diced $LiNbO_3$ ridge waveguides on silicon," J. Opt. **18**, 085503 (2016).
16. M. F. Volk, S. Suntsov, C. E. Rüter, and D. Kip, "Low loss ridge waveguides in lithium niobate thin films by optical grade diamond blade dicing," Opt. Express **24**, 1386–1391 (2016).
17. N. Courjal, B. Guichardaz, G. Ulliac, J.-Y. Rauch, B. Sadani, H.-H. Lu, and M.-P. Bernal, "High aspect ratio lithium niobate ridge waveguides fabricated by optical grade dicing," J. Phys. D: Appl. Phys. **44**, 305101 (2011).
18. T. Umeki, O. Tadanaga, and M. Asobe, "Highly efficient wavelength converter using direct-bonded PPZnLN ridge waveguide," IEEE J. Quantum Electron. **46**, 1206–1213 (2010).